ACS Catalysis

Research Article

pubs.acs.org/acscatalysis

Nature of Ag Species on Ag/γ-Al_2O_3: A Combined Experimental and Theoretical Study

Hua Deng, Yunbo Yu, Fudong Liu, Jinzhu Ma, Yan Zhang, and Hong He*

State Key Joint Laboratory of Environment Simulation and Pollution Control, Research Center for Eco-Environmental Sciences, Chinese Academy of Sciences, Beijing 100085, China

Supporting Information

ABSTRACT: The nature of silver species on Ag/Al_2O_3 catalysts with different silver loadings was studied by photoelectron spectroscopy (XPS) and X-ray absorption near-edge spectroscopy (XANES) and extended X-ray absorption fine structure spectroscopy (EXAFS) combined with theoretical calculation (DFT). On the basis of selective catalytic reduction of NO_x by ethanol experiments, it was found that the optimum silver content varies from 1 wt % to 2 wt %. The supported silver species are predominated by +1 oxidation state ions attached to surface oxygen atoms (Ag−O) under low silver loading of 2 wt %, which play a crucial role during the HC-SCR process. An Ag−Ag shell emerged clearly in analysis of EXAFS data when silver loading was increased to 2 wt %, which was beneficial for low-temperature activity. The theoretical models for $Ag_n^{\delta+}$ species ($1 \le n \le 4$, both ions and oxidized silver clusters) on alumina were consistent with the coordination structure analysis by EXAFS. The predominant silver ions are most likely stabilized at isolated tetrahedral Al sites ($Ag-O-Al_{IVb}$) on the γ-Al_2O_3 (110) surface. However, the most reactive silver ion seems to be anchored on a tricoordinate Al_{III} site ($Ag-O-Al_{III}$). Density of states analysis revealed that the $Ag-O-Al_{III}$ entity might be a very active silver species in terms of the hybridization of Ag, O, and Al orbitals to promote its catalytic activity.

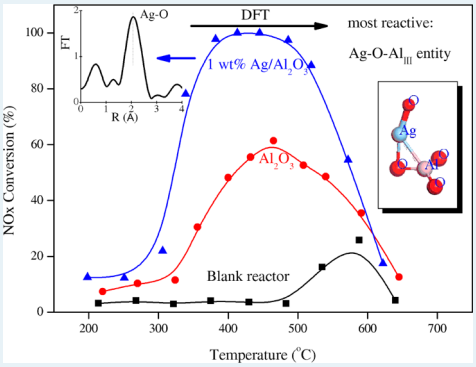

KEYWORDS: *Ag/Al_2O_3, NO_x, SCR, metal−support interaction, XANES, EXAFS, DFT*

1. INTRODUCTION

The potential commercial importance of Al_2O_3-supported silver (Ag/Al_2O_3) catalysts for the selective catalytic reduction of NO_x by hydrocarbons (HC-SCR) in vehicle applications has attracted much attention.[1−6] When using oxygenated hydrocarbons as reductants, particularly ethanol, Ag/Al_2O_3 exhibits high activity even in the presence of SO_2 and H_2O.[7,8] In the presence of trace amounts of H_2, the low temperature activity[9−16] as well as SO_2[17,18] tolerance of Ag/Al_2O_3 can be significantly enhanced when using light hydrocarbons or oxygenated hydrocarbons as reductants. As a result, a great deal of effort has been made to draw a relationship between the structural features of Ag/Al_2O_3 catalysts and their catalytic activity for the SCR of NO_x.

On the basis of characterization by ultraviolet−visible (UV−vis), X-ray adsorption spectroscopy (XAS), and X-ray photoelectron spectroscopy (XPS), it is widely accepted that different kinds of Ag species such as isolated Ag^+ cations, oxidized silver clusters ($Ag_n^{\delta+}$), and metallic silver clusters (Ag_n^0) are present on Ag/Al_2O_3 catalysts as prepared and during HC-SCR.[19−25] Among them, oxidized silver (Ag^+ and/or $Ag_n^{\delta+}$) is believed to be the active species for NO_x reaction by hydrocarbons.[19,21,22,24,25] Kinetic measurements performed by She and Flytzani-Stephanopoulos[19] confirm that Ag^+ cations strongly bonded with the alumina support, possibly present as [Ag−O−Al] entities, are the active sites for SCR of NO_x with methane. On the basis of an elegant short time-on stream in situ spectroscopic transient isotope experimental technique, Burch et al.[26] proposed that the active silver phase and/or its interface with alumina contribute to the adsorption of reactive species like isocyanate during the H_2-assisted octane-SCR over Ag/Al_2O_3. By applying the complementary techniques of kinetic measurements and in situ DRIFTS combined with mass spectrometry, more recently, the key role of oxidized silver species and their interface with alumina in NO_x reduction by ethanol over Ag/Al_2O_3 was quantitatively identified by Yan et al.[27] The results mentioned above suggest that the interaction of silver species with alumina is a key issue for revealing the intrinsic property responsible for high efficiency HC-SCR over Ag/Al_2O_3.

However, the detailed structures of coordinated silver ions or oxidized silver clusters on the γ-Al_2O_3 support surface remain an open question. Furthermore, Zhang and Kaliguine[28] have observed that the activity of Ag/Al_2O_3 catalysts for NO_x reduction by C_3H_6 is significantly influenced by the structure of the support matrix by comparison of various alumina precursors ($Al(OH)_3$ and Al_2O_3). Employing AlOOH as the precursor, the best SCR activity can be achieved.[28,29]

Received: February 26, 2014
Revised: July 1, 2014
Published: July 7, 2014

Nevertheless, the silver loadings for optimum performance are quite different in the findings from each independent group, varying from 2 wt % to 4 wt %.[3,20] A high density of Ag−O−Al species is deemed to be crucial for NO selective reduction to N_2. The surface hydroxyl groups are definitely important in the HC-SCR process both in anchoring silver species and facilitating the formation of vital intermediates like −NCO species. As described above, the local structure of silver species with the support plays a crucial role in the SCR of NO_x by ethanol. Unless the anchored and stabilized sites and structures of these Ag entities on certain surfaces of the γ-Al_2O_3 matrix can be determined, the relationship between the Ag/Al_2O_3 structure and its catalytic performance cannot be understood clearly.

Alumina is one of the most commonly used materials as a catalyst or catalyst support. As for Ag/Al_2O_3 developed for HC-SCR, γ-Al_2O_3-supported samples derived from boehmite (AlOOH) often exhibit high performance, which may originate from a strong interaction between the silver species and the alumina surface.[25,28] Experimental measurement and theoretical investigation confirm that the morphology of γ-Al_2O_3 is directly inherited from the equilibrium morphology of boehmite.[30−32] The γ-Al_2O_3 produced by calcination of boehmite at the optimal temperature mainly consists of exposed (110) surfaces (predominating the total surface area at between 70% to 83%), followed by (100) and (111) surfaces.[33,34] On the three kinds of surfaces, coordinatively unsaturated Al^{3+} sites are quite different, thus giving different abilities for anchoring metal cations and/or particles.[35,36] A study combining experimental measurements such as NMR and density functional theory (DFT) calculation identified coordinatively unsaturated Al^{3+} centers as efficient binding sites for active catalyst phases of platinum on γ-Al_2O_3.[36] According to DFT calculation, Hu et al.[37] investigated the interactions and structures of Pd_{13} and Pt_{13} clusters deposited on (100) and (110) surfaces of γ-Al_2O_3. It was proposed that on the (100) surface, Pt clusters may become negatively charged, whereas Pd clusters remain overall neutral but strongly polarized. This electronic behavior of metal nanoparticles anchored on a given surface of alumina may provide an opportunity to better understand the catalytic reactivity and also to design catalysts with better performance.

As for NO_x abatement, Liu et al.[38] have studied the dissociation of NO on Ag metal clusters without the oxide support by DFT calculation. The possibility that monomeric NO dissociation occurs on bare Ag can be ruled out, but Ag clusters can ionically bond with adsorbates rather than covalently, which finally determines the catalytic performance of silver. Hellman and co-workers[39] have studied NO_x chemistry on Ag_n/Al_2O_3 by first-principles calculations, in which α-Al_2O_3(0001) was selected as a model support. It was proposed that the Ag_n cluster incorporated into the alumina matrix would be in an oxidized state, which is beneficial for NO_x adsorption. As mentioned above, oxidized silver species with high dispersion are active for NO_x reduction by hydrocarbons over Ag/γ-Al_2O_3; however, specific interactions between the surfaces of γ-Al_2O_3 with silver species have not been understood clearly.

In this study, Ag/Al_2O_3 catalysts with different silver loadings were investigated for ethanol-SCR. The chemical state and local structure of silver species on Ag/Al_2O_3 were further studied by XPS, X-ray absorption technology, and DFT calculation. The strong interaction between silver species and the γ-Al_2O_3 support was addressed. It was found that Ag^+ ions were anchored on different sites of the support, among which the Ag−O−Al_{III} ion entity should be the most reactive one based on partial density of states analysis.

2. MATERIALS AND METHODS

2.1. Materials Preparation. Ag/γ-Al_2O_3 catalysts with different silver loadings (0.5, 1, 2, and 4 wt %) were prepared by an impregnation method.[20,40] An appropriate amount of γ-Al_2O_3 (Sigma-Aldrich) was immersed into an aqueous solution of silver nitrate. After stirring for 1 h, the excess water was removed by a rotary evaporator under vacuum at 333 K. Then the sample was calcined in a furnace at 873 K for 3h. For convenience of comparison, the same procedures were followed for pure γ-Al_2O_3.

2.2. Catalytic Measurements. A gaseous mixture of NO (800 ppm), C_2H_5OH (1565 ppm), water vapor (10%), and O_2 (10%) in N_2 balance at a mass flow of 1L min^{-1} was accurately prepared as described in our earlier studies.[27,41] The catalysts were ground and sieved to a size range from 0.25 to 0.42 mm. The concentrations of NO, NO_2, N_2O, NH_3, and CO were analyzed online simultaneously by an FTIR spectrometer (Nicolet Nexus is10). The details of the experimental setup can be found in our earlier work.[27,41] In light of the experimental results, NO_x conversion can be calculated using the following equation:

$$NO_x\ \text{conversion} = \frac{[NO]_{in} + [NO_2]_{in} - [NO]_{out} - [NO_2]_{out}}{[NO]_{in} + [NO_2]_{in}} \times 100\%$$

Meanwhile, a criterion of HC-SCR catalytic materials depends on their selectivity for innocuous N_2. In all the experiments, the concentration of N_2O was negligible. Therefore, the N_2 selectivity could be defined as follows:

$$NO_x\ \text{selectivity} = \frac{[NO]_{in} + [NO_2]_{in} - [NO]_{out} - [NO_2]_{out} - [NH_3]_{out}}{[NO]_{in} + [NO_2]_{in}} \times 100\%$$

2.3. Catalyst Characterization. The X-ray powder diffraction patterns of the various catalysts were collected on a Rigaku D/max-RB X-ray Diffractometer (Japan). The patterns were run with Cu Kα radiation (λ = 1.5406 Å) at 40 kV and 40 mA with a scanning speed of 5°/min. The patterns were taken over the 2θ range from 10° to 90°.

Nitrogen adsorption−desorption isotherms were measured using a Quantachrome Autosorb-1C instrument at 77 K. The specific surface area of the samples was calculated by the Brunauer−Emmett−Teller (BET) method. The volume of pores was determined by the Barrett−Joyner−Halenda (BJH) method from the desorption branches of the isotherms.

XPS analyses were performed using Al Kα radiation with energy of 1486.6 eV and power of 200W. The continuum spectrum was fitted according to Gaussian−Lorentzian line shapes.

The XANES and EXAFS of Ag−K edges were measured in transmission mode at room temperature on the NW10A beamline, Photon Factory, Advanced Ring for pulse X-rays (PF-AR), Institute of Materials Structure Science, High Energy Accelerator Research Organization (IMSS-KEK), Japan. Ag foil and $AgNO_3$ were used as references. The storage ring was operated at 6.5 GeV with 50 mA as an average storage current. The synchrotron radiation beamline was monochromatized

dx.doi.org/10.1021/cs500248a | ACS Catal. 2014, 4, 2776−2784

with a Si (3 1 1) double crystal monochromator, and mirrors were used to eliminate higher harmonics. Before measurements, all samples were crushed and sieved to 200 mesh or finer and then diluted with flour powder at appropriate ratios and pressed into thin disks.

XANES and XAFS data were analyzed by the REX2000 program (Rigaku Co.). XANES spectra were normalized with edge height and then the first order derivatives were taken to compare the variation of absorption edge energies. EXAFS oscillation $\chi(k)$ was extracted using spline smoothing and weighted by k^3 to compensate for the diminishing amplitude in the high k range. The filtered k^3 weighted $\chi(k)$ was transformed to R space in the k range of 2 to 9 $Å^{-1}$ with a Hanning function window. The structural parameters of the series of catalysts were obtained through curve fitting procedures using FEFF8.4 code.[42]

2.4. DFT Calculations. All calculations are performed using Materials Studio (MS) Modeling CASTEP from Accelrys. Periodic boundary conditions in the generalized gradient approximation (GGA) using the Perdew–Wang (PW91) function were applied in our cases. All initial parameters had been checked by convergence tests. The electron–ion interaction was described by the ultrasoft potential in reciprocal space. A tight convergence of the plane-wave expansion was obtained with a kinetics energy cutoff of 400 eV. Because the most abundant exposed surface of γ-Al_2O_3 is (110) termination, the dehydrated (110) surface of γ-alumina was established according to previously proved models.[31,32,37] The optimized unit cell size was 8.068 × 8.413 Å for the (110) surface, which is consistent with reported values. The inter slab distance was maintained at 15 Å to avoid inter slab interactions in the periodic systems. Eight-layer-thick slabs (formula $Al_{32}O_{48}$) were constructed in this study. A test calculation showed the models had negligible energy variance with layers increasing from six to seven. Base on this result, only the bottom two layers were kept fixed during the calculations. On the basis of the convergence test for k-point sampling, the k-point set of (2 × 2 × 1) was used for the Al_2O_3 (110) surface.

The Ag ion and $Ag_n^{\delta+}$ cluster were modeled both in isolated state and supported on the alumina (110) surface, in which isolated Ag ions and clusters were optimized in a 20 × 20 × 20 Å cubic cell. The Brillouin-zone k-point mesh sampling was restricted to gamma point. Several models were constructed to simulate the supported silver alumina catalysts according to a method derived from others' works.[38,39] In order to compare the structure stability, the adsorption energy of Ag species on the γ-Al_2O_3 support was calculated as follows:

$$E_{ad} = E_{adsorbate+surface} - (E_{surface}+E_{adsorbate})$$

The flow of charges was estimated by Mulliken population analysis. The electronic structures were analyzed in terms of density of states (DOS) and partial density of states (PDOS).

3. RESULTS AND DISCUSSION

3.1. Catalyst Characterization. Ag/Al_2O_3 catalysts with different silver loadings were characterized by BET and XRD measurements. As shown in Table 1, the pure Al_2O_3 exhibited a BET surface area of 167.3 m^2/g. An increase in silver loading resulted in a decrease in surface area to some degree, which was accompanied by a gradual decrease in pore volume and an increase in average pore diameter. Only the γ-Al_2O_3 phase, but no metallic Ag or Ag_2O phase, was detected by XRD measurement as the silver loading increased from 0 to 4 wt % (Figure S1). This suggests that the silver species were highly dispersed on the surface of γ-Al_2O_3. In this case, XPS, XANES, and DFT technologies were further used to reveal the chemical states of the silver, and the detailed information can be found in sections 3.3–3.5.

Table 1. Structure Parameters of Ag/Al_2O_3 Catalysts with Different Silver Loadings Derived from N_2 Physisorption Results

sample	BET (m^2/g)	pore volume (mL/g)	mean pore diameter (nm)
Al_2O_3	167.3	0.28	6.72
0.5% Ag/Al_2O_3	160.9	0.28	7.03
1% Ag/Al_2O_3	148.5	0.27	7.22
2% Ag/Al_2O_3	151.8	0.25	6.56
4% Ag/Al_2O_3	145.2	0.26	7.21

3.2. Catalytic Activity of Ag/Al_2O_3 Catalyst. The conversion of NO_x by ethanol and N_2 selectivity over Ag/Al_2O_3 catalysts are displayed in Figure 1. It can be clearly seen in Figure 1A that only 25% NO_x conversion can be achieved in the case of the blank reactor at temperature of 600 °C. With pure γ-Al_2O_3 as catalyst, the highest conversion of 60% was obtained at almost 500 °C. Increasing the silver content from 0 to 1 wt % significantly enhanced the NO_x conversion, the latter of which exhibited NO_x conversion above 97% within a temperature window of 100 °C (382–486 °C). Increasing

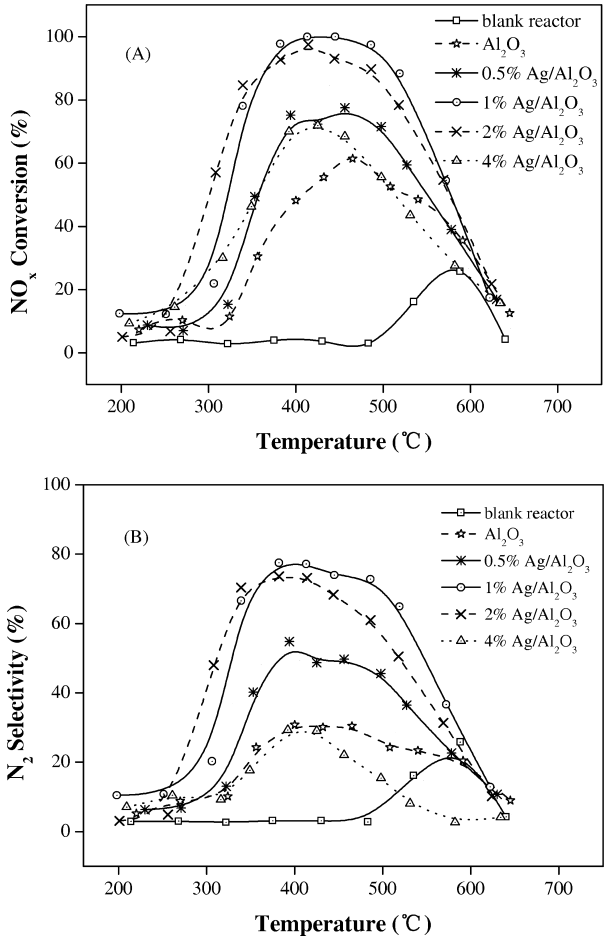

Figure 1. NO_x conversion (A) and N_2 selectivity (B) for SCR by C_2H_5OH over Ag/Al_2O_3 catalysts with different silver loadings.

dx.doi.org/10.1021/cs500248a | ACS Catal. 2014, 4, 2776–2784

silver content to 2 wt % further promoted NO_x conversion in the low temperature region but sacrificed the NO_x reduction at temperatures above 400 °C. Further increasing the silver content to 4 wt % significantly decreased the NO_x conversion in the whole temperature range. In our previous studies,[20,21,27,40,41] boehmite (CHINALCO, China) was selected as a precursor to prepare Ag/Al_2O_3. In that case, the Ag/Al_2O_3 with 4 wt % silver loading exhibited the best performance for HC-SCR, confirming the crucial role of the support and/or its precursor in determining the performance of Ag/Al_2O_3 catalysts.[28] As for Ag/γ-Al_2O_3 developed by other groups, the optimum silver loading is often about 2 wt %,[2,43−46] which is in agreement with our results presented here.

NH_3 is a common byproduct in ethanol-SCR processes.[41,47,48] Because only a negligible amount of N_2O was detected in this study, the N_2 selection depended mainly on the formation of NH_3 within the active temperature window. Figure 1B compares the detailed N_2 selectivity among all reaction conditions. In the case of the blank reactor, 25% N_2 selectivity can be obtained, which is equal to its NO_x conversion value. With pure γ-Al_2O_3 as a catalyst, a maximum N_2 selectivity of 30% was obtained. Increasing the silver content from 0 to 2 wt % significantly enhanced the N_2 selectivity, among which the sample with 1 wt % Ag exhibited the highest N_2 selectivity, about 76% in a 100 °C temperature window (382−486 °C). The N_2 selectivity order for 0.5, 1, and 2 wt % samples can be described as 1 wt % >2 wt % >0.5 wt %. It is noteworthy that the NH_3 yields are the same, 23%, for the three samples. Further increasing silver content to 4 wt % significantly lowered the N_2 selectivity, with the promotion of the NH_3 selectivity to 40%.

3.3. Chemical State of Ag Species. The valence states of supported Ag were characterized by XPS, with the results shown in Figure 2. The peaks of the Ag $3d_{5/2}$ binding energy

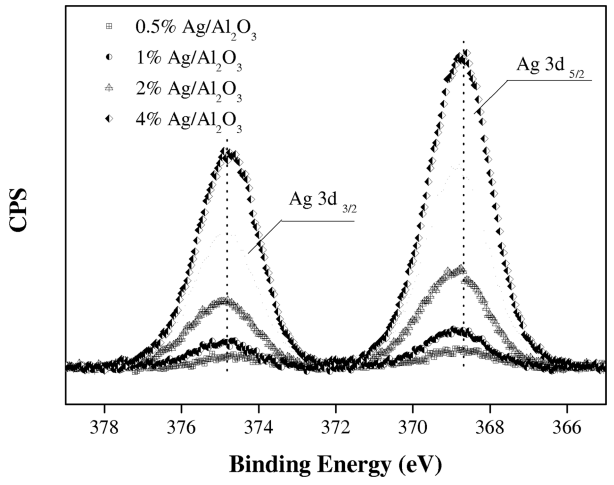

Figure 2. XPS spectra of the Ag 3d level for Ag/γ-Al_2O_3 catalysts with different silver loadings.

for all samples appeared at around 368.0−368.6 eV, which is consistent with the values ranging from 367.8 to 368.4 eV reported in previous studies.[21,49,50] On the basis of the binding energy values, we can tentatively state that the silver atoms on the surface might be in the oxidized state.[21] As for the samples with silver loading around 0.5−1 wt %, the peaks of Ag $3d_{5/2}$ exhibited high symmetry. On increasing the content of silver to 4 wt %, the surface silver content was observed to increase substantially. It is well-known that it is difficult for XPS characterization to reveal the precise chemical state of silver species. Thus, XAS (X-ray adsorption spectrum) technology was used to learn the chemical state of silver species on Ag/Al_2O_3 catalysts.

In order to understand the precise chemical state of supported silver, the Ag−K XANES of samples with different silver loadings, $AgNO_3$, and Ag foil were investigated (Figure 3). It can be clearly seen in Figure 3A that the Ag/γ-Al_2O_3

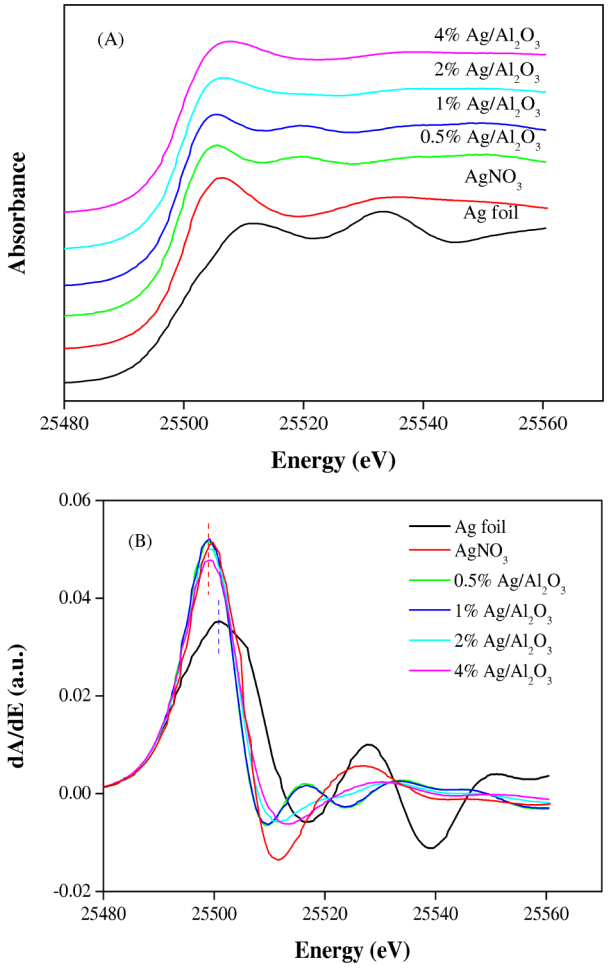

Figure 3. Normalized Ag−K XANES (A), first-order derivatives of Ag−K XANES in Ag/γ-Al_2O_3 catalysts with different silver loadings (B).

catalysts and $AgNO_3$ show similar Ag−K absorption edge energy, while being lower than that of Ag foil. It has been reported that Ag has lower binding energy with increasing oxidation state due to its core-level photoemission.[21,50] According to this empirical rule, supported silver species for all samples are mostly close to the +1 oxidation state, just like Ag^+ ion in $AgNO_3$ solid. As shown in Figure 3B, the first-order derivative peak appeared at 25499.19 eV for Ag^+ in $AgNO_3$. In addition, other first derivative peaks for 0.5 wt %, 1 wt %, 2 wt %, 4 wt % Ag/Al_2O_3 catalysts were observed at 25499.19, 25498.89, 25499.19, 25499.78 eV, respectively. However, the corresponding absorption edge energy for the Ag−K edge in Ag foil appeared at 25500.97 ev. These findings are consistent with the above-mentioned XPS results and confirm that in the Ag/Al_2O_3 samples, Ag is present mainly in the +1 oxidation state

dx.doi.org/10.1021/cs500248a | ACS Catal. 2014, 4, 2776−2784

below 2 wt %. Increasing silver content to 4 wt %, the silver species exhibited a partial metal state like that in Ag foil.

3.4. Local Structure of Ag Species. Figure 4 shows the Fourier transforms of k^3-weighted EXAFS oscillations at the Ag K-edge. A bond distance in the range of 1.75−2.5 Å was observed over all Ag/Al_2O_3 samples, which can be assigned to an Ag−O shell. A peak at ca. 2.7 Å could be due to the backscattering from adjacent silver atoms.[23,24,51] For all Ag/Al_2O_3 samples, the peak of the Ag−O shell is predominant, which is consistent with previous XPS and XANES results, suggesting that silver species are mainly in the oxidized state. An Ag−Ag shell starts to emerge clearly with silver loading increasing from 2 wt % to 4 wt %.

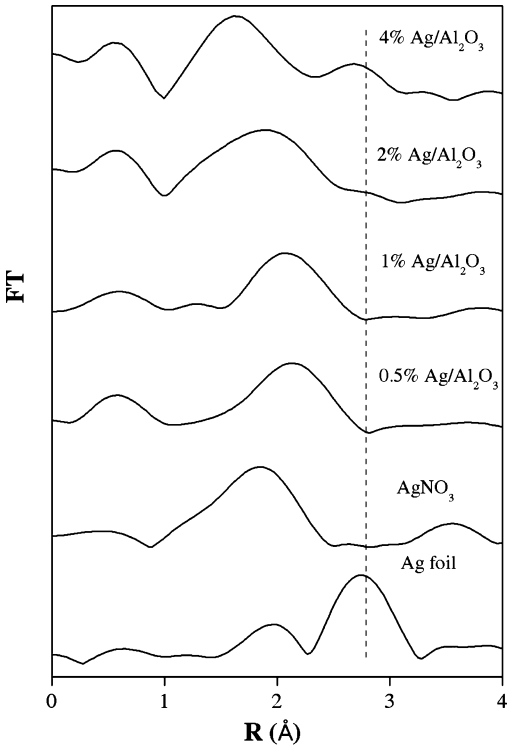

Figure 4. EXAFS spectra of Ag/Al_2O_3 catalysts with various Ag loadings, $AgNO_3$, and Ag foil.

In order to obtain the local coordination structure of Ag species on Ag/Al_2O_3 catalysts, curve fitting was performed, with the results shown in Figure S2, Figure S3 in Supporting Information and Table 2. Only an Ag−O shell was found on 0.5 and 1 wt % Ag/Al_2O_3 catalysts in this study, where the Ag−O bond distance and coordination number are 2.5 Å and 2.6−3.0 respectively. Other studies[24,25] also have reported a similar Ag−O distance of 2.48 Å based on EXAFS measurements for calcined silver alumina catalysts. In our study, on increasing the silver content to 2 wt %, the Ag−Ag shell with bond distance of 2.7 Å started to emerge. Other studies[24,25] also showed similar EXAFS results, where the Ag−Ag bond distances for Ag/Al_2O_3 catalysts were 2.69 to 2.74 Å. This suggests that our obtained structure parameters are in good agreement with previous studies.[23−25] Further increasing our silver loading to 4 wt %, the coordination number of Ag−Ag increased to 1.5 but that of Ag−O decreased to 1.9. Combining these results with catalytic efficiency data, the 1 wt % sample dominated by the Ag−O shell exhibited the best NO_x reduction performance among all samples, indicating oxidized silver ions (Ag^+) may play the real role of active site. In the case of the 2 wt % sample, promotion of low temperature (250−300 °C) catalytic performance and depression of performance in the high temperature range (above 400 °C) were found as shown in Figure 1, which is in good agreement with other reports.[22,52] As suggested by Nam et al., the presence of silver clusters ($Ag_n^{\delta+}$ and Ag_n^0) promotes the partial oxidation of hydrocarbons to produce active oxygenated species at low temperatures, which is thus beneficial for NO_x reduction at low temperatures, but they are not preferable in the high temperature region.[22,53] However, further increasing the silver loading causes a decrease in the NO_x reduction efficiency over the whole temperature range. Based on EXAFS analysis, a conclusion can be drawn that silver ions (Ag^+) most likely act as the active site during the reduction process of NO_x by ethanol. However, the detailed structures of coordinated silver ions or silver clusters on the γ-Al_2O_3 matrix surface are still unknown.[23−25] In the following section, the DFT method was adopted to simulate their surface and electronic structures.

3.5. DFT Calculation. As described above, the surface (110) is the main exposed facet,[33,34] which accounted for about 70−83% of all surface area.[31,32] Furthermore, the observed reactivity of "activated" alumina might have originated from the major (110) termination of alumina as suggested by Wischert et al.,[54] because the tricoordinate Al_{III} and tetracoordinate Al_{IV} sites present on this facet may correspond to the "defect" sites.[54] On the basis of these two important factors, the fully dehydrated γ-Al_2O_3 (110) unit cell with a size of 8.068 × 8.413 Å was selected as the support matrix, in which there are four Al atoms with different coordination. The most abundant (110) surface exposes one tricoordinate Al_{III} and two kinds of

Table 2. Curve Fitting Results of Ag−K EXAFS for Different Ag/Al_2O_3 Samples (Corrected by the Crystallographic Data of $AgNO_3$ and Ag Foil)

sample	shell	R (Å)	CN	σ^2(10^{-3} Å^2)	dE	R factor (%)
Ag foil	Ag−Ag	2.8 (0.1)	12.3 (2.3)	13	0.5	0.03
$AgNO_3$	Ag−O	2.4 (0.1)	6.3 (0.4)	16	6.1	2.92
0.5% Ag/Al_2O_3	Ag−O	2.5 (0.1)	3.0 (0.5)	13	6.7	2.98
	Ag−Ag					
1% Ag/Al_2O_3	Ag−O	2.5 (0.1)	2.6 (0.5)	11	6.0	0.95
	Ag−Ag					
2% Ag/Al_2O_3	Ag−O	2.4 (0.1)	2.6 (1.3)	28	−2.4	0.67
	Ag−Ag	2.7 (0.1)	1.3 (0.7)	23	−10.6	
4% Ag/Al_2O_3	Ag−O	2.3 (0.1)	1.9 (0.2)	23	−6.6	1.51
	Ag−Ag	2.7 (0.1)	1.5 (0.4)	24	−7.3	

dx.doi.org/10.1021/cs500248a | ACS Catal. 2014, 4, 2776−2784

tetracoordinate Al_{IV} sites (namely, Al_{IVa} and Al_{IVb}). Because an impregnation method was used to synthesize Ag/Al_2O_3 catalysts, surface hydroxyl groups are reasonably abundant. According to Wischert et al.,[54] the adsorption energy for hydroxyl groups adsorbed on different Al sites including Al_{III} and/or Al_{IV} sites was quite similar at high coverage. We postulate that each Al site has equal possibility to desorb hydroxyl groups and anchor silver ions in this case. Thus, the Al_{III}, Al_{IVa}, and Al_{IVb} (Figure 5A) were selected as the silver

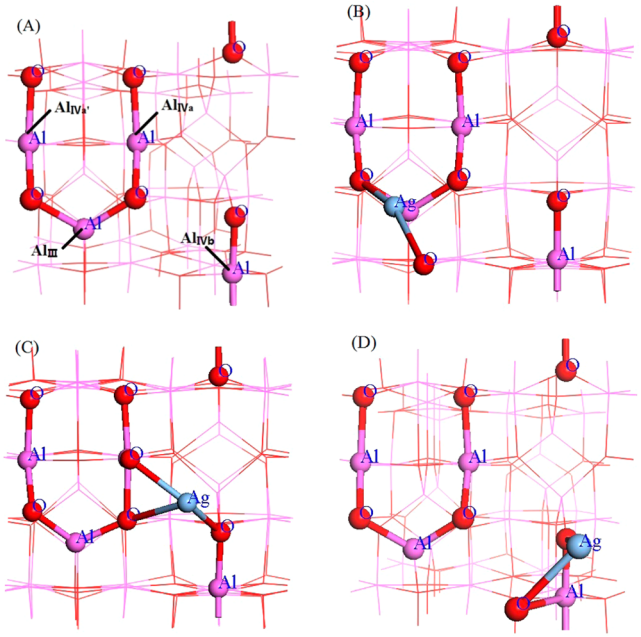

Figure 5. Fully dehydroxylated (110) termination of γ-Al_2O_3 (A) AgO on (110) surface model 1 (Ag^+−O-Al_{III}) (B) AgO on (110) surface model 2 (Ag^+−O-Al_{IVa}) (C) AgO on (110) surface model 3 (Ag^+−O-Al_{IVb}) (D).

anchoring sites to construct the basic models, denoted as model 1, 2, 3, respectively. AgO was used as the isolated silver ion unit, which indicates that Ag^+ ion exchanges with H^+ from hydroxyl groups of different Al sites, respectively. The adsorption of the AgO unit on different locations of the fully dehydrated γ-Al_2O_3 (110) surface is presented in Figure 5. The adsorption energy and structural parameters are summarized in Table 3.

It can be clearly seen in Table 3 that model 3 (Ag^+−O-Al_{IVb}) has the lowest total energy among all Ag^+ ion models. Our model fully dehydrated gamma-Al_2O_3 unit cell has three kinds of Al site on the suface, namly, Al_{III}, Al_{IVa}, and Al_{IVb}. AgO unit can be anchored on these sites, forming model 1 (Ag-O-Al_{III}), model 2 (Ag-O-Al_{IVa}), and model 3 (Ag-O-Al_{IVb}), respectively. These three models can be ascribed as Ag^+ ion species on Al_2O_3 surface. Wheareas, other models in Table 3 can be labeled as Ag clusters on Al_2O_3 surface. It is only reasonable to compare model 3 in the zone of silver ion species models. Thus models 4 to 6 are excluded in this comparison. The order of stability of all models studied can be described as model 3> model 2> model 1. The DFT calculations indicated that the most stable model 3 exhibits the highest positive silver Mulliken charge, near the +1 oxidation state, which is consistent with earlier XPS and XANES results. The model 1 (Ag^+−O-Al_{III} site), with the lowest positive silver Mulliken charge, is relatively energetically unfavorable.

It is well-known that EXAFS only presents an "averaged" coordination structure, especially for surface-supported catalysts. Using the EXAFS experiment, as shown in Table 2, we found that the average Ag−Ag coordination number is less than two. This suggests that the local structures of silver species are predominated by Ag ion species, but $Ag_n^{\delta+}$ clusters are also important in the HC-SCR process.[19,21,22,24,25] In order to discern the differences between silver ion and cluster, the possible silver cluster structures were studied. The silver cluster ($Ag_n^{\delta+}$) size factor was considered by increasing the number of silver atoms from two to four (refs 23, 26, 28, 52, 55−57) based on the model 3 structure at the Al_{IVb} site due to its energetically favorable nature, as formerly suggested. Thus, silver cluster models with silver atoms varying from 2, 3, to 4 were constructed in the study, denoted as models 4, 5, 6, respectively. All the models are exhibited in Figure 6. The average bond distance, coordination number, and Mulliken charge are also listed in Table 3.

It can be clearly seen from Table 3 that the structural parameters of DFT models were highly consistent with the EXAFS experiments. For example, model 1 (Ag^+−O-Al_{III}), 2 (Ag^+−O-Al_{IVa}), and 3 (Ag^+−O-Al_{IVb}) described an idealized Ag/Al_2O_3 catalyst that is exclusively dominated by Ag^+ ion, where the Ag−O bond distance and coordination numbers vary from 2.3 to 2.5 Å and 2.0 to 3.0 respectively. Combined with EXAFS experiments, the 0.5 and 1 wt % Ag/Al_2O_3 catalysts both can be labeled as Ag^+ ion-dominated catalysts, because only Ag−O shells were observed, as shown in Table 2. Their Ag−O bond distances were both 2.5 Å, and coordination numbers varied from 2.6 to 3.0. Other silver cluster structures were also found to be in good agreement in both EXAFS measurements and DFT calculation. Thus, DFT models follow the experimental observations, and we can deduce the structure−activity relationship theoretically. For model 4 ($Ag_2^{\delta+}$−O-Al_{IVb}), the $Ag_2^{\delta+}$ formed a $(AgO)_2$ short belt structure on the Al_2O_3 surface without Ag−Ag bonding. Combining the structure and Mulliken charge, this suggests that the $(AgO)_2$ short belt is a derivative member of the

Table 3. DFT Calculated Adsorption Energies, Structural Parameters, and Mulliken Charge

	structural parameters $_{av}$				adsorption energy (eV)	Mulliken charge (e)$_{av}$
	Ag−O		Ag−Ag			
	R (Å)	N	*R* (Å)	N		
model 1 (Ag^+−O-Al_{III})	2.5	2.0			−1.56	0.57
model 2 (Ag^+−O-Al_{IVa})	2.3	3.0			−2.44	0.65
model 3 (Ag^+−O-Al_{IVb})	2.4	2.0			−2.88	0.73
model 4 ($Ag_2^{\delta+}$−O-Al_{IVb})	2.3	2.0			−3.03	0.52
model 5 ($Ag_3^{\delta+}$−O-Al_{IVb})	2.3	2.0	2.7	2.0	−3.15	0.27
model 6 ($Ag_4^{\delta+}$−O-Al_{IVb})	2.4	1.7	2.8	3.0	−4.92	0.25

dx.doi.org/10.1021/cs500248a | ACS Catal. 2014, 4, 2776−2784

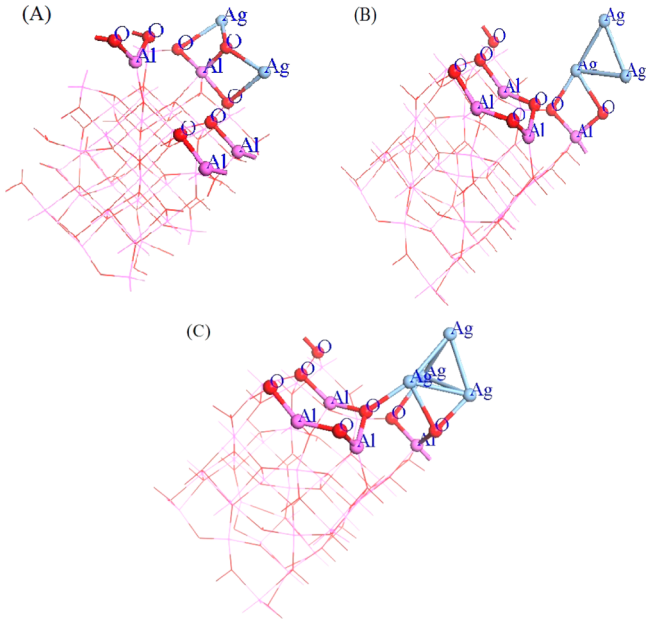

Figure 6. $Ag_2^{\delta+}$ cluster on (110) surface model 4 ($Ag_2^{\delta+}$−O-Al_{IVb}) (A), $Ag_3^{\delta+}$ cluster on (110) surface model 5 ($Ag_3^{\delta+}$−O-Al_{IVb}) (B), $Ag_4^{\delta+}$ cluster on (110) surface model 6 ($Ag_4^{\delta+}$−O-Al_{IVb}) (C).

predominant silver ion species. The shape of $Ag_3^{\delta+}$ for model 5 ($Ag_3^{\delta+}$−O-Al_{IVb}) was a triangle stood on its head on the matrix. It is clear that the silver atom bonds with each other no longer spread into AgO units on the surface as in model 4. Meanwhile, the Ag−Ag shell can be observed. This indicated that the Ag−Ag shell in EXAFS experiments might be composed of $Ag_n^{\delta+}$ clusters with $n \geq 3$. As for model 6 ($Ag_4^{\delta+}$−O-Al_{IVb}), the cluster $Ag_4^{\delta+}$ was stabilized as a tetrahedron structure on the (110) surface. The silver atoms self-organized to form a polyhedron with the most metallic chemical state among all the silver clusters in this study. From the Mulliken charge analysis, we found that the silver atom exhibits an increasingly metallic state as the Ag−Ag coordination number increases as shown in Table 3. These are different from the silver ion species (Ag^+) anchored on Al_2O_3 by means of exchanging with H^+ in hydroxyl. As a result of the strong repulsive effect among silver ions (Ag^+), silver clusters like the Ag-trimer may interact with the alumina surface by excess silver solution ripening directly on anchored silver ions or on the Al_2O_3 surface.

3.6. Electronic Structure of Silver Species. In order to understand the nature of silver species, models 1 to 6, including the fully dehydrated γ-Al_2O_3 (110) surface model, were investigated by means of band structure and density of states (DOS and PDOS). DOS is a powerful tool to analyze the energy levels of slabs. The region between the top of the valence band and the bottom of conduction band, which are similar to the HOMO and LUMO in molecules, is related to the reactivity. It is well-known that a system with a small band gap is more reactive than one with a high value.[58−60] As suggested by band structure analysis, the band gap for the γ-Al_2O_3 (110) surface was 3.499 eV, while the band gaps for models 1 to 6 were 0.521, 1.301, 1.413, 1.501, 0.738, and 1.531 eV respectively (Figure S4). It is clearly evident that the band gap becomes narrower because of the supported silver. Thus, the Ag/Al_2O_3 catalyst is more reactive than the support. Among all models, model 1 (Ag^+−O-Al_{III}) seems to be most reactive and model 5 ($Ag_3^{\delta+}$−O-Al_{IVb}) should be the second, both of which likely play key roles in the HC-SCR process, especially the Ag^+−O-Al_{III} structure. Other works[19,27] based on experimental results suggest that Ag^+ ions are active sites. For instance, She and Flytzani-Stephanopoulos[19] confirmed that Ag^+ cations are the active sites for SCR of NO_x with methane by leaching catalysts and comparing activation energies. On the basis of kinetic measurements and in situ DRIFTS combined with mass spectrometry, we also believe Ag^+ cations are the active sites in NO_x reduction by ethanol over Ag/Al_2O_3.[27]

To reveal the reactivity mechanism for different silver species structures, the DOS results of surface (110), model 1(Ag^+−O-Al_{III}) and model 5 ($Ag_3^{\delta+}$−O-Al_{IVb}) were determined and

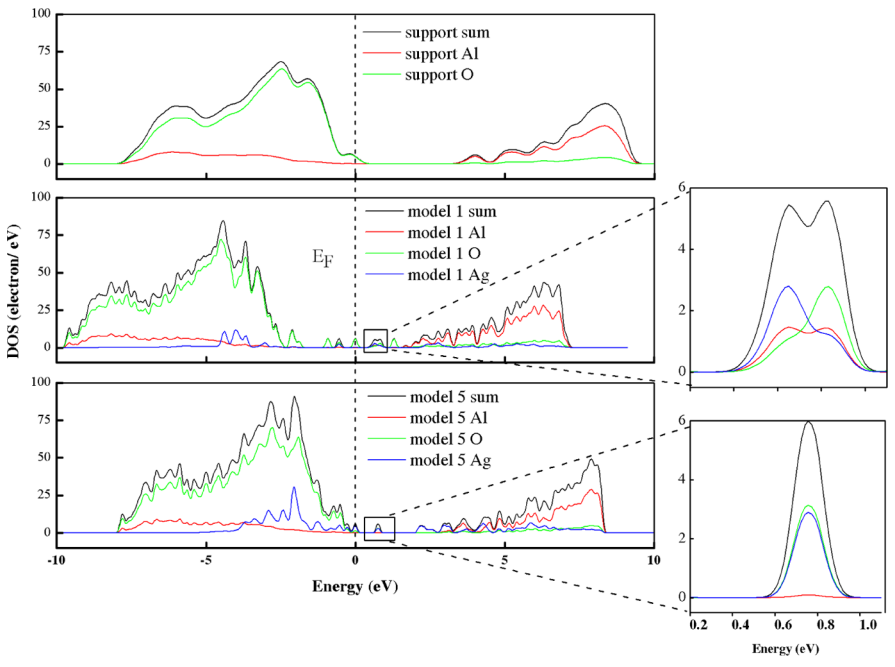

Figure 7. Density of states (DOS) of Al, O, and Ag atoms in support Al_2O_3 (110) surface, model 1, and model 5.

dx.doi.org/10.1021/cs500248a | ACS Catal. 2014, 4, 2776−2784

plotted in Figure 7. From comparison of the support, model 1 and model 5, we can see that the valence band is mainly composed of oxygen orbitals, whereas the conduction band is composed of Al orbitals. The reason that model 1 (Ag^+−O-Al_{III}) has the highest chemical reactivity can be ascribed to the orbital mixing among Ag, O, and Al states at 0.65 and 0.85 eV, as shown in Figure 7. The detailed PDOS results (Figure S5A) show that the Ag−O−Al_{III} interaction can be attributed to the bonding among silver s orbitals, oxygen p orbitals, and aluminum s and p orbitals. The Ag−O−Al_{III} entity is also mainly ionic because most of the oxygen p orbital density is below the E_F (Fermi surface energy) and most of aluminum s and p orbital and silver s orbital density is above the E_F (Figure S6). On the contrary, other models such as models 2, 3, 4, and 6 (Figure S5) do not have strong Ag, O, Al interactions from mixing their orbitals at the bottom of the conduction band to improve their reactivity. Thus, we can postulate that the strong interaction between metal (silver species) and support determines the catalytic performance. As for model 5 ($Ag_3^{\delta+}$−O-Al_{IVb}), the $Ag_3^{\delta+}$ cluster should be more reactive than other silver cluster models. The key factor can be ascribed to the Ag−O interaction as shown in Figure 7. The PDOS results (Figure S5E) revealed there is orbital hybridization among the silver s orbital, and especially the d orbital, with the oxygen p orbital at 0.75 eV, which eventually reduces the energy gap, whereas other silver cluster models, like model 4 ($Ag_2^{\delta+}$−O-Al_{IVb}, Figure S5D), do not mix the silver d orbital with the oxygen p orbital owing to the deficiency of silver atoms in the cluster. But increasing the number of silver atoms to 4 is not beneficial for reactivity either; take model 6 ($Ag_4^{\delta+}$−O-Al_{IVb}, Figure S5F), for example, because the silver atoms agglomerating with each other, the Ag−O bond becomes weak, and the hybridization between the silver s orbital and the oxygen p orbital is negligible in the lower conduction band. Thus, silver cluster species may have an optimum number of silver atoms in terms of catalytic performance, and $Ag_3^{\delta+}$ should be the most active among the silver cluster species studied. Other literature[23,25,26] also suggest that the average size of silver clusters is about three silver atoms under reaction conditions. Generally, the H_2 effect during HC-SCR can partially be attributed to the structure change of the active site. Transforming from Ag^+ cations to oxidized silver clusters may actually take place under reaction conditions. However, the nature of the H_2 effect remains an open debate.

It was well-known that oxidized silver species ($Ag_n^{\delta+}$, $1 \le n \le 4$) are possibly more active than metal silver species on Ag/Al_2O_3 catalyst for HC-SCR as mentioned before.[20,21] In this study, we learned the detailed structure and valence charge of silver ions and clusters. On the basis of ethanol-SCR activity testing and catalyst structure analysis such as EXAFS characterization, we found that oxidized silver species, especially silver ions, play a crucial role in reduction of NO_x. With the aid of DFT calculation, we built idealized Ag/Al_2O_3 catalyst models. Strong consistencies in terms of structure and activity between experimental and theoretical observations were found. The electronic structures revealed that the activity of silver ions originates from the Ag, O, Al orbital mixing. The interaction between metal and support is addressed. In our further study, effort will be devoted to the subject of chemical activities, especially on the activation of HC reductants related to the main silver species.

4. CONCLUSIONS

Several Ag/Al_2O_3 catalysts were prepared with different silver loadings on the same pure γ-Al_2O_3 support. For ethanol-SCR, it was found that the optimum silver content is 1 wt % to 2 wt %, on which silver species are predominated by an oxidation state close to Ag^+ ions, serving as the active sites for NO_x reduction. The Ag−Ag shell can be observed clearly, along with promotion of catalytic performance only at low temperature, when silver loading is increased to 2 wt %. DFT simulations of silver local structures, including silver ions and oxidized silver clusters, were in good agreement with experimental characterization, in terms of structure and activity. The sample with 1 wt % Ag/Al_2O_3, exclusively predominated by silver ions, exhibited the best reduction performance, which was also confirmed by idealized silver ion catalyst models. The predominant silver ions are most likely stabilized at the Al_{IVb} site on the Al_2O_3 (110) surface. However, the most reactive silver ion seems to be anchored on the Al_{III} site. DOS revealed that the mixing of orbitals in the Ag−O−Al_{III} entity significantly decreases the band gap and likely enhances its reactivity. An opportunity for better understanding the intrinsic property of strong interaction between Ag^+ ions and the γ-Al_2O_3 support is supplied by analyzing the nature of silver species on Ag/Al_2O_3 catalysts.

■ ASSOCIATED CONTENT

Supporting Information

The XRD spectrum and EXAFS fitting results of different Ag/Al_2O_3 samples are displayed in Figure S1, Figure S2, and Figure S3, respectively. Band structure and density of state study of Ag/Al_2O_3 models are presented in Figure S4 to S6. This material is available free of charge via the Internet at http://pubs.acs.org.

■ AUTHOR INFORMATION

Corresponding Author

*E-mail: honghe@rcees.ac.cn.

Notes

The authors declare no competing financial interest.

■ ACKNOWLEDGMENTS

The work was supported by the National Natural Science Foundation of China (21373261 and 21177142) and the National High Technology Research and Development Program of China (863 Program, 2013AA065301).

■ REFERENCES

(1) Burch, R.; Breen, J. P.; Meunier, F. C. *Appl. Catal., B* **2002**, *39*, 283−303.
(2) Shimizu, K.I.; Satsuma, A. *Phys. Chem. Chem. Phys.* **2006**, *8*, 2677−2695.
(3) He, H.; Zhang, X. L.; Wu, Q.; Zhang, C. B.; Yu, Y. B. *Catal. Surv. Asia* **2008**, *12*, 38−55.
(4) Li, J. H.; Ke, R.; Li, W.; Hao, J. M. *Catal. Today* **2008**, *139*, 49−58.
(5) Granger, P.; Parvulescu, V. I. *Chem. Rev.* **2011**, *111*, 3155−3207.
(6) Kamolphop, U.; Taylor, S. F. R.; Breen, J. P.; Burch, R.; Delgado, J. J.; Chansai, S.; Hardacre, C.; Hengrasmee, S.; James, S. L. *ACS Catal.* **2001**, *1*, 1257−1262.
(7) Miyadera, T. *Appl. Catal., B* **1993**, *2*, 199−205.
(8) Wang, J.; He, H.; Xie, S. X.; Yu, Y. B. *Catal. Commun.* **2005**, *6*, 195−200.
(9) Satokawa, S. *Chem. Lett.* **2000**, 394−395.

(10) Satokawa, S.; Shibata, J.; Shimizu, K. I.; Satsuma, A.; Hattori, T. *Appl. Catal., B* **2003**, *42*, 179−186.
(11) Burch, R.; Breen, J. P.; Hill, C. J.; Krutzshch, B.; Konrad, K.; Jobson, E.; Cider, L.; Eranen, K.; Klingstedt, F.; Lindfors, L. E. *Top. Catal.* **2004**, 19−25.
(12) Arve, K.; Backman, H.; Klingstedt, F.; Eranen, K.; Murzin, D. Y. *Appl. Catal., A* **2006**, *303*, 96−102.
(13) Arve, K.; Backman, H.; Klingstedt, F.; Eranen, K.; Murzin, D. Y. *Appl. Catal., B* **2007**, *70*, 65−72.
(14) Satokawa, S.; Shibata, J.; Shimizu, K. I.; Satsuma, A.; Hattori, T.; Kojima, T. *Chem. Eng. Sci.* **2007**, *62*, 5335−5337.
(15) Zhang, X. L.; He, H.; Ma, Z. C. *Catal. Commun.* **2007**, *8*, 187−192.
(16) Zhang, X. L.; Yu, Y. B.; He, H. *Appl. Catal., B* **2007**, *76*, 241−247.
(17) Shimizu, K. I.; Higashimata, T.; Tsuzuki, M.; Satsuma, A. *J. Catal.* **2006**, *239*, 117−124.
(18) Shimizu, K. I.; Tsuzuki, M.; Satsuma, A. *Appl. Catal., B* **2007**, *71*, 80−84.
(19) She, X.; Stephanopoulos, M. F. *J. Catal.* **2006**, *237*, 79−93.
(20) He, H.; Yu, Y. B. *Catal. Today* **2005**, *100*, 37−47.
(21) He, H.; Li, Y.; Zhang, X. L.; Yu, Y. B.; Zhang, C. B. *Appl. Catal., A* **2010**, *375*, 258−264.
(22) Kim, M. K.; Kim, P. S.; Baik, J. H.; Nam, I. S.; Cho, B. K.; Oh, S. H. *Appl. Catal., B* **2011**, *105*, 1−14.
(23) Breen, J. P.; Burch, R.; Hardacre, C.; Hill, C. J. *J. Phys. Chem. B* **2005**, *109*, 4805−4807.
(24) Shimizu, K. I.; Tsuzuki, M.; Kato, K.; Yokota, S.; Okumura, K.; Satsuma, A. *J. Phys. Chem. C* **2007**, *111*, 950−959.
(25) Korhonen, S. T.; Beale, A. M.; Newton, M. A.; Weckhuysen, B. M. *J. Phys. Chem. C* **2011**, *115*, 885−896.
(26) Chansai, S.; Burch, R.; Hardacre, C.; Breen, J.; Meunier, F. *J. Catal.* **2011**, *281*, 98−105.
(27) Yan, Y.; Yu, Y. B.; He, H.; Zhao, J. J. *J. Catal.* **2012**, *293*, 13−26.
(28) Zhang, R. D.; Kaliaguine, S. *Appl. Catal., B* **2008**, *78*, 275−287.
(29) He, H.; Yu, Y. B.; Li, Y.; Wu, Q.; Zhang, X. L.; Zhang, C. B.; Shi, X. Y.; Song, X. P. *Chin. J. Catal.* **2010**, *31*, 491−501.
(30) Krokidis, X.; Raybaud, P.; Gobichon, A. E.; Rebours, B.; Euzen, P.; Toulhoat, H. *J. Phys. Chem. B* **2001**, *105*, 5121−5130.
(31) Digne, M.; Sautet, P.; Raybaud, P.; Euzen, P.; Toulhoat, H. *J. Catal.* **2002**, *211*, 1−5.
(32) Digne, M.; Sautet, P.; Raybaud, P.; Euzen, P.; Toulhoat, H. *J. Catal.* **2004**, *226*, 54−68.
(33) Nortier, P.; Fourre, P. *Appl. Catal.* **1990**, *61*, 141−160.
(34) Alvarez, L. J.; Sanz, J. F.; Capltan, M. J.; Centeno, M. A.; Odrlozola, J. A. *J. Chem. Soc., Faraday Trans.* **1993**, *89*, 3623−3628.
(35) Kwak, J. H.; Mei, D. H.; Yi, C. W.; Kim, D. H.; Peden, C. H. F.; Allard, L. F.; Szanyi, J. *J. Catal.* **2009**, *261*, 17−22.
(36) Kwak, J. H.; Hu, J. Z.; Mei, D. H.; Yi, C. W.; Kim, D. H.; Peden, C. H. F.; Allard, L. F.; Szanyi, J. *Science* **2009**, *325*, 1670−1673.
(37) Hu, C. H.; Chizallet, C.; Mager-Maury, C.; Corral-Valero, M.; Sautet, P.; Toulhoat, H.; Raybaud, P. *J. Catal.* **2010**, *274*, 99−110.
(38) Liu, Z. P.; Jenkins, S. J.; King, D. A. *J. Am. Chem. Soc.* **2004**, *126*, 7336−7340.
(39) Hellman, A.; Gronbeck, H. *J. Phys. Chem. C* **2009**, *113*, 3674−3682.
(40) He, H.; Zhang, C. B.; Yu, Y. B. *Catal. Today* **2004**, *90*, 191−197.
(41) Yu, Y. B.; Zhao, J. J.; Yan, Y.; Han, X.; He, H. *Appl. Catal., B* **2013**, *136−137*, 103−111.
(42) Ankudinov, A. L.; Ravel, B.; Rehr, J. J.; Conradson, S. D. *Phys. Rev. B* **1998**, *58*, 7565−7576.
(43) Lindfors, L. E.; Eranen, K.; Klingstedt, F.; Murzin, D. Y. *Top. Catal.* **2004**, *28*, 185−189.
(44) Bion, N.; Saussey, J.; Haneda, M.; Daturi, M. *J. Catal.* **2003**, *217*, 47−58.
(45) Arve, K.; Hernandez Carucci, J. R.; Eranen, K.; Aho, A.; Murzin, D. Y. *Appl. Catal., B* **2009**, *90*, 603−612.
(46) Johnson, W. L.; Fisher, G. B.; Toops, T. J. *Catal. Today* **2012**, *184*, 166−177.
(47) Miyadera, T. *Appl. Catal., B* **1997**, *13*, 157−165.
(48) Can, F.; Flura, A.; Courtois, X.; Royer, S.; Blanchard, G.; Marecot, P.; Duprez, D. *Catal. Today* **2011**, *164*, 474−479.
(49) Tjeng, L. H.; Meinders, M. B. J.; Ghijsen, J. E. J.; Sawatzky, G. A. *Phys. Rev. B* **1990**, *41*, 3190−3199.
(50) Kannisto, H.; Ingelsten, H. I.; Skoglundh, M. *J. Mol. Catal. A: Chem.* **2009**, *302*, 86−96.
(51) Shimizu, K. I.; Shibata, J.; Yosida, H.; Satsuma, A.; Hattori, T. *Appl. Catal., B* **2001**, *30*, 151−162.
(52) Shibata, J.; Takada, Y.; Shichi, A.; Satokawa, S.; Satsuma, A.; Hattori, T. *J. Catal.* **2004**, *222*, 368−376.
(53) Yoon, D. Y.; Park, J. H.; Kang, H. C.; Kim, P. S.; Nam, I. S.; Yeo, G. K.; Kil, J. K.; Cha, M. S. *Appl. Catal., B* **2011**, *101*, 275−282.
(54) Wischert, R.; Laurent, P.; Coperet, C.; Delbecq, F.; Sautet, P. *J. Am. Chem. Soc.* **2012**, *134*, 14430−14449.
(55) Sazama, P.; Capek, L.; Drobna, H.; Sobalik, Z.; Dedecek, J.; Arve, K.; Wichterlova, B. *J. Catal.* **2005**, *232*, 302−317.
(56) Satsuma, A.; Shibata, J.; Shimizu, K. I.; Hattori, T. *Catal. Surv. Asia* **2005**, *9*, 75−85.
(57) Shibata, J.; Shimizu, K. I.; Takada, Y.; Shichi, A.; Yoshida, H.; Satokawa, S.; Satsuma, A.; Hattori, T. *J. Catal.* **2004**, *227*, 367−374.
(58) Hoffman, R. *Rev. Mod. Phys.* **1988**, *60*, 601−628.
(59) Liu, Z. M.; Ma, L. L.; Junaid, A. S. M. *J. Phys. Chem. C* **2010**, *114*, 4445−4450.
(60) Calatayud, M.; Minot, C. *J. Phys. Chem. C* **2007**, *111*, 6411−6417.